A Novel Approach to Solvation Time Scale in Nonpolar Solvents via Instability of Solvent Density Modes

R. Biswas*,† and J. Chakrabarti

Department of Chemical, Biological and Macromolecular Sciences, S. N. Bose National Centre for Basic Sciences, JD Block, Salt Lake City, Kolkata 700 098, India

Received: July 27, 2007; In Final Form: September 24, 2007

We perform linear stability analysis of solvent density modes in the presence of nonpolar solute−solvent interaction in a nonpolar solvent. The dominant instability given by the maximum positive eigenvalue of the stability matrix provides the time scale of the solvent rearrangement around a solute. Our theory predicts two long time scales for both in normal nonpolar and supercritical fluids. We discuss the existing experimental results on nonpolar solvation dynamics in light of our prediction.

I. Introduction

The distribution of solvent molecules around a solute is of fundamental importance in chemical sciences, for it governs the rate of reactions in solution phase. The molecular processes underlying the rate-determining factors can be probed by the solvation time[1−7] that measures the time scale of solvent response to an excitation of a dissolved solute. Experimental, theoretical, and simulation techniques have been extensively used to understand the solvation time in solvents of different polarity as well as diverse thermodynamic conditions. The time-dependent response of a solvent is usually expressed in terms of the solvent response function, $S(t) = [\Delta E(t) - \Delta E(\infty)]/[\Delta E(0) - \Delta E(\infty)]$, where $\Delta E(t)$ is the time-dependent solvation energy gap with respect to the ground state of the solute.[2−6] Consider a solute in equilibrium with a bath of solvent particles. Let the interaction between the solute (u) at **R** and a solvent (v) at **r** in the ground state of the solute be $V_{uv}^{gs}(\mathbf{r} - \mathbf{R})$. Also, assume that the solute−solvent interaction becomes $V_{uv}^{ex}(\mathbf{r} - \mathbf{R})$ upon solute excitation that leads to solvent rearrangement before a new equilibrium state is established. Here, $\Delta E(t) = \int d\mathbf{r}[V_{uv}^{ex}(\mathbf{r} - \mathbf{R})\rho(\mathbf{r},t) - V_{uv}^{gs}(\mathbf{r} - \mathbf{R})\rho_{gs}(\mathbf{r})]$, where $\rho(\mathbf{r},t)$ is the time-dependent solvent density around the solute, and $\rho_{gs}(\mathbf{r})$ is that in equilibrium with the solute in its ground state. The time $t = 0$ refers to that immediately after the solute excitation.

Since the nonpolar interactions largely govern the long-time dynamics of solvent, it is inherently interesting to study the nonpolar solvation dynamics. Nonpolar solvation dynamics involves changes in the shape and/or size of the solute upon photoexcitation.[8−9] Experiments on solvation dynamics of a dipolar solute in non-dipolar solvents report a very fast inertial and a couple of longer diffusive time scales.[4] The theories of solvation dynamics are based on the linear response of coupled density and momentum fields,[2−3] where $S(t)$ is expressed as a time-correlation function of $\Delta E(t)$, averaged over an equilibrium ensemble. In such theories,[1−3] the nonpolar solvation dynamics is determined by the relaxation of the solvent dynamic structure factor, which explains the bimodal decay of $S(t)$ with time scales comparable to the inertial time scale and the smaller of the two long-time components observed in experiments.[4]

Here we present a theoretical approach that can account for both of the long-time components observed in experimental studies of nonpolar solvation dynamics. Our approach is based on the highly nonlinear hydrodynamic equation (NHE) governing the time dependence of $\rho(\mathbf{r},t)$.[6] The present theoretical framework avoids the nontrivial task of solving the full nonlinear equation but can yield qualitative understanding of both the solvation time scale and the length scale of the inhomogeneity in solvent distribution. We perform linear stability analysis[10] of the NHE governing $\rho(\mathbf{r},t)$. The density mode associated with the maximum positive frequency provides the time scale of solvent rearrangement around the solute, and the inverse of the corresponding wave vector gives the length scale of inhomogeneity of the solvent distribution.

The flow of the paper is as follows: We discuss the theoretical framework in section II. We apply our analysis to incompressible fluids in section III and to compressible fluids in section IV. We conclude the paper in section V.

II. Theory

The continuity equation for $\rho(\mathbf{r},t)$ is given by[11] $\partial_t\rho(\mathbf{r},t) + \nabla\cdot\mathbf{j} = 0$, where $\mathbf{j}$ is the solvent particle current density. Here we consider the overdamped limit in order to capture the diffusive dynamics. In the overdamped limit, $\mathbf{j} = -D\rho(\mathbf{r},t)\nabla(\beta\mu)$, where β is the inverse of the Boltzmann constant times the absolute temperature (k_BT). D is the Stokes' diffusion coefficient ($= k_BT/3\pi\eta\sigma \approx 10^{-4}$ cm^2 s^{-1} at room temperature) of a solvent molecule with diameter σ in a medium of viscosity η, μ is the chemical potential, and $\beta\mu = \delta\beta F[\rho(\mathbf{r},t)]/\delta\rho(\mathbf{r},t)$, with $\beta F[\rho(\mathbf{r},t)]$ being the free energy cost of creating nonequilibrium solvent density inhomogeneity over the ground-state equilibrium solvent distribution. In equilibrium of the bulk solvent, the free energy cost for creating density inhomogeneity $\rho(\mathbf{r})$ over a uniform state of density ρ_0 is given by the density functional free energy,[11] $\beta F^{eq}[\rho(\mathbf{r})] = \int d\mathbf{r}\rho(\mathbf{r})[\ln\{(\rho(\mathbf{r})/\rho_0)\} - 1] - (1/2)\int d\mathbf{r}d\mathbf{r}'c(\mathbf{r} - \mathbf{r}')[\rho(\mathbf{r}) - \rho_0][\rho(\mathbf{r}') - \rho_0]$. $\beta F^{eq}[\rho(\mathbf{r})]$ is truncated to the second order in the correlation, given by $c(\mathbf{r} - \mathbf{r}')$, the static correlation of the bulk solvent, assuming the change in density, $\rho(\mathbf{r}) - \rho_0 \ll \rho_0$. The bulk phase diagram is obtained by minimizing $\beta F^{eq}[\rho(\mathbf{r})]$ with respect to $\rho(\mathbf{r})$ using the appropriate $c(\mathbf{r} - \mathbf{r}')$ as input. Here we model $\beta F[\rho(\mathbf{r},t)]$ as a generalization of $\beta F^{eq}[\rho(\mathbf{r})]$ to nonequilibrium density fluctua-

* Corresponding author. E-mail: ranjit@bose.res.in.
† Also at UNANST, S. N. Bose National Centre for Basic Sciences.

10.1021/jp075949n CCC: $37.00
Published on Web 11/14/2007

SCHEME 1: Scattering Geometry[a]

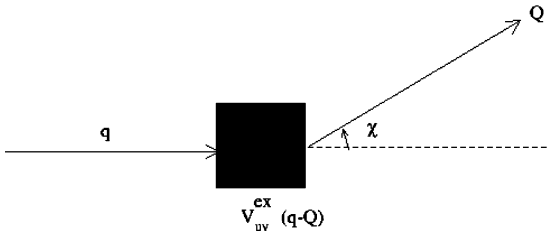

[a] χ is the angle between the incoming wave vector **q** and the outgoing wave vector **Q**. The black box indicates the scattering potential.

tions, as in the dynamical density functional theory (DFT)[12−15] $\beta F[\rho(\mathbf{r},t)] = \int d\mathbf{r}\rho(\mathbf{r},t) \times [\ln(\rho(\mathbf{r},t)/\rho_{gs}(\mathbf{r})) - 1] - (1/2) \int d\mathbf{r}d\mathbf{r}' c(\mathbf{r} - \mathbf{r}')[\rho(\mathbf{r},t) - \rho_{gs}(\mathbf{r})] \times [\rho(\mathbf{r}',t) - \rho_{gs}(\mathbf{r}')] + \beta \int d\mathbf{r} V_{uv}^{ex}(\mathbf{r} - \mathbf{R})$-$[\rho(\mathbf{r},t) - \rho_{gs}(\mathbf{r})]$, with $c(\mathbf{r} - \mathbf{r}')$ being the same as in the static case.[16] The nonequilibrium density fluctuations are measured with respect to solvent distribution in the ground state. We introduce the ground-state inhomogeneity, $\delta\rho_{gs}(\mathbf{r})$ and the nonequilibrium density fluctuations $\delta\rho(\mathbf{r},t)$ as follows: $\rho_{gs}(\mathbf{r}) = \rho_0 + \delta\rho_{gs}(\mathbf{r})$ and $\rho(\mathbf{r},t) = \rho_{gs}(\mathbf{r}) + \delta\rho(\mathbf{r},t)$. We calculate **j** to linear order in $\delta\rho(\mathbf{r},t)$ by expanding $\beta F[\rho(\mathbf{r},t)]$ to quadratic order in $\delta\rho(\mathbf{r},t)$. Let both $V_{uv}^{gs}(\mathbf{r} - \mathbf{R})$ and $V_{uv}^{ex}(\mathbf{r} - \mathbf{R})$ have the same spatial symmetry as that of the bulk solvent, so that a unique wave vector **q** specifies the modes for both $\delta\rho_{gs}(\mathbf{r})$ and $\delta\rho(\mathbf{r},t)$: $\delta\rho_{gs}(\mathbf{r}) = \sum_{\mathbf{q}}\rho_{gs}(\mathbf{q}) \exp[i\mathbf{q}\cdot\mathbf{r}]$ and $\delta\rho(\mathbf{r},t) = \sum_{\mathbf{q},\omega}\rho(\mathbf{q},\omega) \exp[i\mathbf{q}\mathbf{r} + \omega t]$, with ω being the frequency. The linearized hydrodynamic equation can be written as $\omega\sigma^2 D^{-1}\rho(\mathbf{q},\omega) = \Omega_{\mathbf{q},\mathbf{Q}}\rho(\mathbf{Q},\omega)$, where the stability matrix, $\Omega_{\mathbf{q},\mathbf{Q}} = -q^2[1 - \rho_0 c(\mathbf{q}) - \rho_{gs}(\mathbf{q})c(\mathbf{q})]\delta[\mathbf{q} - \mathbf{Q}] - \sum_{\mathbf{Q}}\mathbf{q}\cdot[\mathbf{q} - \mathbf{Q}]V_{uv}^{ex}(\mathbf{q} - \mathbf{Q})$. Within the equilibrium DFT,[17] the linearized mode $\rho_{gs}(\mathbf{q}) = V_{uv}^{gs}(\mathbf{q})S(\mathbf{q})$, where the solvent static structure factor $S(\mathbf{q}) = [1 - \rho_0 c(\mathbf{q})]^{-1}$. Here the second term describes the following scattering process: A solvent density mode with **q** is scattered to that with **Q** at an angle χ, shown in Scheme 1, with an amplitude proportional to $V_{uv}^{ex}(\mathbf{p})$, where $\mathbf{p} = \mathbf{q} - \mathbf{Q}$. The positive eigenvalues of $\Omega_{\mathbf{q},\mathbf{Q}}$ indicate the growing modes, the maximum positive being the dominant one.

We apply the present theory to solvation in a nonpolar isotropic solvent where $c(\mathbf{q}) = c(q)$, where $q = |\mathbf{q}|$. For nonpolar solute−solvent interactions, $\rho_{gs}(\mathbf{q})$ and $\rho(\mathbf{q},\omega)$ depend on q. $V_{uv}^{gs}(|\mathbf{r} - \mathbf{R}|) = V_{LJ}(|\mathbf{r} - \mathbf{R}|) = 4\epsilon[(\sigma/|\mathbf{r} - \mathbf{R}|)^{12} - (\sigma/|\mathbf{r} - \mathbf{R}|)^6]$, with ϵ being the ground-state solute−solvent interaction strength. We further take $\beta V_{uv}^{ex}(|\mathbf{r} - \mathbf{R}|) = UV_{LJ}(|\mathbf{r} - \mathbf{R}|)$, where $U = f\beta$, with f being the ratio of the solute−solvent interaction in the excited state to that in the ground state. The unit length in our calculations, $\sigma = 4A^0$, and the time unit, $\tau_D = \sigma^2/6D \approx 4$ ps. We take the solute fixed at $\mathbf{R} = 0$. The upper panel of Figure 1 shows that the scattering amplitude, $-U^{-1}V_{uv}^{ex}(p^*)$, as a function of $p^* = p\sigma$, has a peak around $p^* = 0$, with half width at the half-maximum, $\delta p^* \sim 1$. $V_{uv}^{gs}(q^*)$ shows similar dependence on q^*. The peak at $p^* = 0$ indicates that the solute−solvent interaction contributes a maximum for the low momentum transfer processes. Further, because of isotropy, the scattering amplitude depends on q^* and Q^*. For instance, for scattering $Q^* = q^*$, the scattered mode has wave vector q^* but rotated by χ with respect to the incident $\mathbf{q}^*$ so that $p^* = 2q^* \sin(\chi/2)$. For low p^*, $V_{uv}^{ex}(p^*)$ is expanded as $V_{uv}^{ex}(p^*) = V_0 - p^{*2}V_2$, where $V_0 = 4\pi \int dr r^2 V_{uv}^{ex}(r)$ and $V_2 = 4\pi \int dr r^4 V_{uv}^{ex}(r)$. This scattering term, after integrating over χ, contributes to the diagonal term. The off-diagonal terms are given by the scattering for $q^* \neq Q^*$.

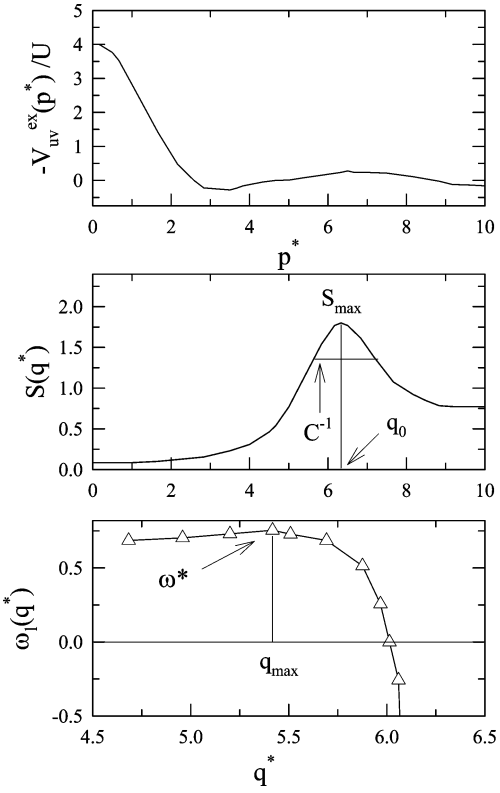

Figure 1. Upper panel: The Fourier transform of the solute−solvent interaction term $V_{uv}^{ex}(p^*)/U$ as a function of wave vector p^* (scaled by the solvent diameter σ). Middle panel: Solvent static structure factor, $S(q^*)$ as a function of q^* at $\rho_r = 1.5$ and $T_r = 1.06$. S_{max} at the ordering wave vector q_0 and the width C^{-1} have been indicated. Lower panel: Frequency $\omega_l(q^*)$ as a function of wave vector q^*. The following parameters have been used for the calculation of $\omega_l(q^*)$: $S_{max} = 2$ and $C = 10$. Note that the modes are damped for $q^* > 6.0$. The maximum positive frequency ω^* and its location q_{max} have been indicated.

III. Incompressible Fluids

Let us first consider an incompressible high-density liquid for which $S(q^*)$ possesses a strong peak[11] at $q^* = q_0 = 2\pi$. About the peak, $S(q^*)$ is parametrized as $[S_{max} + C(q^{*2} - q_0^2)^2]$. S_{max} is the peak value, and C is the inverse of the peak width. The solvent static structure factor $S(q^*)$ at a representative solvent density ($\rho_r = 1.5$, $T_r(= T/T_c) = 1.06$) is shown in the middle panel of Figure 1. Since the solvent structure is largely governed by the $S(q^*)$ peak, we consider the modes with $q^* \sim q_0$. Further, we restrict to small p^* by integrating χ up to $\chi_0 = \delta p^*/2\pi \ll 1$ to capture the dominant scattering contribution. The resulting frequency (diagonal element) in scaled units is given by $\omega_l(q^*) = -q^{*2}[1/S(q^*) - (S(q^*) - 1)V_{uv}^{gs}(q^*)] - \sqrt{(8\pi)}\,[q^{*2}V_0\chi_0^4/8 - q^{*4}V_2\chi_0^6/24]$, shown in the lower panel of Figure 1. A density mode with q^* is unstable, namely, it will grow with a time scale of $[\omega_l(q^*)]^{-1}$, if $\omega_l(q^*) > 0$. On the other hand, the modes, having $\omega_l(q^*) < 0$, will decay with time. $\omega_l(q^*)$ has a maximum positive value, ω^*, at a nontrivial q_{max}, indicating the dominant instability with time $\tau^* = 1/\omega^*$ and inhomogeneity in the length scale of solvent distribution $\sim 2\pi/q_{max}$. We find that $\tau^* \approx 0.7$ and $q_{max} \approx 5.5$ for $U = 4$ ($f = 3$ and $\beta\epsilon = 1/3$), close to the experimental solute−solvent interaction strength.[18] The term q_{max} corresponds to a length scale $\sim\sigma$. Hence, $\tau = \tau^* \tau_D$ (~ 3 ps) is the solvent rearrangement time in the first solvation shell and is comparable to experimental nonpolar solvation time.[4] Hence, we identify τ as the solvation time scale.

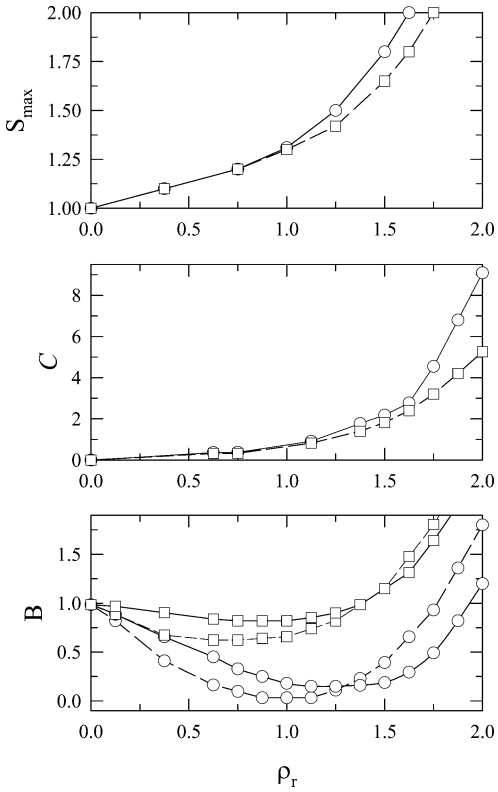

Figure 2. Upper panel: The density dependence of the peak value of the solvent static structure factor (S_{max}) at $T_r = 1.06$ (circles) and 3.0 (squares). Middle panel: The density dependence of the inverse width (C) at $T_r = 1.06$ (circles) and 3.0 (squares). All the joining lines are guides to the eyes. Lower panel: The inverse compressibility B for different ρ_r at $T_r = 1.06$ (circles) and 3.0 (squares). The joining solid line denotes the MF treatment, and the dashed line represents the PREOS (for further details, see text).

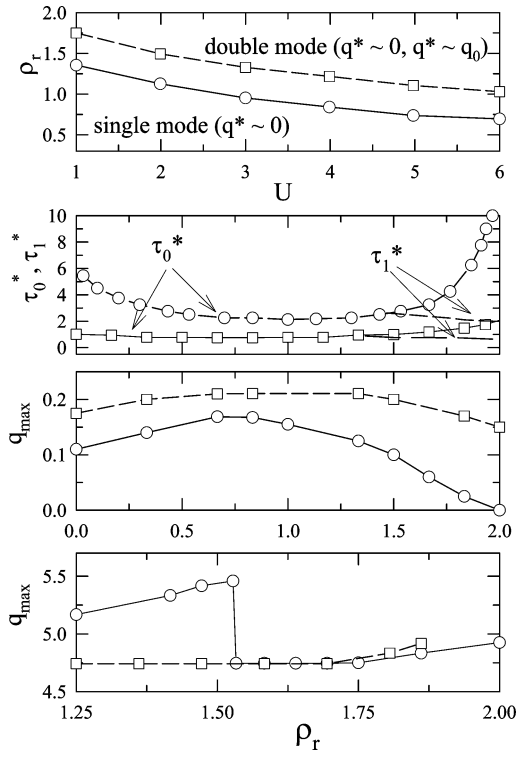

Figure 3. Upper panel: Instability diagram in the ρ_r versus U plane: The regions of instability with a single mode ($q^* \sim 0$) and double modes ($q^* \sim 0$ and $q^* \sim q_0$) are differentiated by the squares ($T_r = 3.0$) and the circles ($T_r = 1.06$), respectively. The joining lines are guides to the eyes. First middle panel: τ_0^* (solid line joining squares for $T_r = 3.0$ and dashed line joining circles for $T_r = 1.06$) and τ_1^* (long-dashed line for $T_r = 3.0$ and short-dashed line for $T_r = 1.06$) as functions of ρ_r for $U = 4$. Second middle and lower panels: The solvent density dependence of q_{max} for the $q^* \sim 0$ mode and for the $q^* \sim q_0$ mode, respectively (solid lines joining circles for $T_r = 1.06$ and dashed line joining squares for $T_r = 3.0$).

IV. Compressible Fluids

Next we consider solvation in a compressible Lennard-Jones (LJ) solvent with interaction $\beta V_{LJ}(r)$ between two solvent molecules separated by r. LJ systems have a gas−liquid critical point[11] due to the long-range attraction, given by $T_c = 1.32$ and $\rho_c = 0.39$, obtained from the divergence of the compressibility B^{-1} in the empirical Peng−Robinson equation of state (PREOS).[19] The estimated critical point is in good agreement with the simulations on LJ systems.[20] The density dependence of S_{max} at two different temperatures ($T_r = 1.06$ and 3.0) is presented in the upper panel of Figure 2. The density-dependent inverse width (C) and inverse compressibility (B) are respectively shown in the middle and lower panels of Figure 2. These density-dependent quantities are also determined at two different temperatures, $T_r = 1.06$ (circles) and 3.0 (squares). The lower panel of Figure 2 further shows that the inverse compressibility from the PREOS compares well with B [$\propto 1/S(q^* = 0)$], obtained from $c(q^*)$ using Percus−Yevick (PY) closure for the short-range repulsion and the mean field (MF) approximation for the long-range attraction.[11] Note that such a construction of $c(q^*)$ using the PY and MF approximations are known to be valid for near-critical fluids as well.[21] Further, the estimation of the critical temperature and density within the MF treatment is close to those obtained from the PREOS. Hence, we use the MF treatment for $c(q^*)$ to understand nonpolar solvation and compare our results with experimental systems. Note that $T_r = 1.06$ corresponds to a temperature slightly above the T_c, which falls in the domain of supercritical fluid (SCF).[22−23] For a given T_r, D is scaled as $\tilde{D} = DT_r$ and $U = (\epsilon/k_B T_c)(f/T_r)$. We incorporate modes with both small ($q^* \sim 0$) and finite ($q^* \sim q_0$) wave vectors to include the effects of compressibility and finite wave-vector solvent correlations, respectively. The diagonal element corresponding to $q^* \sim 0$ is given as follows: $\omega_g(q^*) = -q^{*2}[B - (B^{-1} - 1)V_{uv}^{gs}(q^*) - 2\sqrt{2\pi}\, V_0] + (64/\sqrt{18\pi})q^{*4}V_2$. This has been obtained by expanding $V_{uv}^{gs}(q^*)$ in the low q^* and considering a weak q^* dependence of $S(q^*)$ in this regime of q^* (see middle panel of Figure 1). The diagonal element for $q^* \sim q_0$ is $\omega_l(q^*)$, whose expression has already been given in section III. The off-diagonal term[24] is $(q^* q_0 V_{uv}^{ex}(q_0))/4\pi^2$.

We consider two temperatures ($T_r = 1.06$ and 3.0) for compressible fluids. First we illustrate the scenario at $T_r = 3$. The upper panel of Figure 3 shows different instabilities encountered in the U versus ρ_r plane. The line joining the squares shows the instability diagram at $T_r = 3$. Below a critical ρ_r (ρ_r^c, squares), the small wave-vector modes become unstable, while the finite wave-vector modes are damped. However, for $\rho_r > \rho_r^c$, both the small and finite wave-vector modes are unstable with a slow (τ_0^*) and a fast (τ_1^*) time scale, respectively. The density dependence of these time scales is depicted in the first middle panel of Figure 3 (line joining squares and long-dashed line, respectively). The upper panel of this figure (Figure 3) indicates that ρ_r^c decreases with U, implying that the solute−solvent interaction facilitates the instability of the solvent density modes. For $U = 4$, we find that $\rho_r^c \approx 1.3$. The density dependence of the compressibility mode ($q_{max} \ll 1$) and that of the ordering wave-vector mode ($q_{max} \approx q_0$, for $\rho_r > \rho_r^c$) are

shown in the second middle and lower panels of Figure 3 (lines joining squares).

At $\rho_r = 2.0$ and $U = 4$, $q_{max} \approx 4.8$, implying a length scale of $\sim 1.3\sigma$ and an instability time scale τ_1^* of ~ 2.5, shown by the long-dashed line in the middle panel of Figure 3. τ_1^* is comparable to τ^* for incompressible fluids, indicating that the corresponding instability is driven by the finite wave-vector solvent correlations. τ_0^* (line joining squares) is not sensitive to ρ_r for $\rho_r < \rho_r^c$ ($\tau_0^* \approx 1$ for $U = 4$). τ_0^* in this range can be retrieved by considering the $q \sim 0$ mode alone without any off-diagonal coupling. This instability is thus governed by finite compressibility, arising via the long-range attraction in the solvent−solvent interaction. For $\rho_r > \rho_r^c$, τ_0^* becomes slower and differs appreciably from τ_1^*. The growth of the first solvation shell is enhanced by the increase in liquid correlations as density increases. However, diffusion of the solvent particles becomes slower as density increases, leading to the slowing down of τ_0^*. The emergence of the double mode is thus a manifestation of an interplay between compressibility and finite wave-vector solvent correlations. Recent experiments[4] suggest that the solvation dynamics of a dipolar probe in non-dipolar solvents exhibits multiple time scales: a very short time scale ($\sim$200 fs) due to solvent inertial effects and two relatively longer time scales (2−4 ps and >10 ps). The fast inertial time scales cannot be retrieved in overdamped dynamics, but the longer time scales ($\tau_0 = \tau_0^* \tau_D \approx 10$ ps and $\tau_1 = \tau_1^* \tau_D \approx 2.4$ ps) agree well with experiments.[4]

The interplay between the compressibility and the short-range liquid structure is expected to be very strong for solvation in SCF.[22−23] The instability diagram at $T_r = 1.06$ has been shown by the line joining the circles in the upper panel of Figure 3. The first middle panel of Figure 3 (line joining circles and the short-dashed line) shows the time scales. As in the high temperature, there is a single mode ($q^* \sim 0$), dominated by the compressibility effects for the low ρ_r, and an additional faster mode ($q^* \sim q_0$) appears for sufficiently large ρ_r ($\rho_r > \rho_r^c \approx 1.5$ for $U = 4$) as a result of strong liquid correlations. Because of enhanced liquid correlations at low temperature, ρ_r^c(circles) for a given U, is smaller than that at high temperature. q_{max} for the SCF is shown in the second middle panel and the lower panel of Figure 3 (lines joining circles). The length scale for the correlation-driven mode ($q_{max} \approx 5$) is comparable to that in ref 25. Note that τ_0^* has a broad minimum for ρ_r, where B also shows the minimum (lower panel of Figure 2). τ_1^* scales roughly as temperature as in $\tilde{D}$, implying that τ_1^* even in SCF is governed by the short-range repulsion[26] in $\beta V_{LJ}(r)$. However, the long-range attraction in $\beta V_{LJ}(r)$ is crucial for observing two solvation time constants at long times. At $\rho_r = 2.0$, $\tau_0 \approx 60$ ps and $\tau_1 \approx 8$ ps. The shorter time scale is in good agreement with experiments in supercritical fluoroform using *trans*-4-(dimethylamino)-4′-cyanostilbene (DCS) as the probe that reports a long-time solvation time scale of $\sim$10 ps in comparable density ranges.[27] However, the experiments using DCS do not report any other longer time scale. On the other hand, experiments using a longer lifetime probe such as C153 in the same fluid at similar solvent conditions report solvation with a long time scale of $\sim$50 ps, albeit without any faster long-time component.[28] While DCS is a shorter lifetime probe, experiments with C153 employed techniques with a time resolution of $\sim$25 ps. These might be reasons for detecting single long time scales in the above experiments.

It may be worthwhile to compare our results to the existing simulation results.[29−38] Although the molecular dynamics (MD) simulations on nonpolar solvation dynamics extract the inertial fast time scale and a fast diffusive time scale ($\sim$1 ps), none of them report the slow diffusive time scale ($\sim$10 ps), found in experiments and obtained in the present study. In the SCF, ref 6 reports a time scale of 10 ps using MD simulations, which is comparable to the faster diffusive time scale obtained from our analysis. These simulations do not find the slow diffusive mode. Since our study indicates that this slow time scale is associated with the compressibility effects, the simulations to extract such a time scale may require a much larger system size.

V. Conclusion

In summary, we show that the dominant instability of the solvent density modes provides a good qualitative picture of the molecular processes underlying solvation dynamics. The dominant instability describes the growth of solvent density modes in response to the change in the solute−solvent interaction. We extract two time constants at long times as observed in the experiments on solvation dynamics in non-dipolar solvents due to interplay between the compressibility and short-range correlations of solvent. The present theory is based on the following approximations: (i) the ground-state solvent inhomgeneity is small; (ii) the correlations are truncated at the second order; and (iii) only the specific modes with wave vectors $q^* \sim 0$ and $q^* \sim q_0$ have been retained in the stability analysis. Approximation (i) is reasonable for weak solute−solvent interaction in the ground state. Approximation (ii) is routinely used in any density functional calculation because of lack of knowledge on the higher order correlations.[1−3] Approximation (iii) has been used considering the solvent structure, having finite compressibility and a finite wave-vector correlation peak at $q^* \sim q_0$. It may be interesting to investigate the consequences of relaxing some of these approximations. The full solvent response function, $S(t)$ cannot be extracted from the present linearized treatment, because the calculation of $S(t)$ requires the amplitudes of the density modes, which depend on the nonlinear terms as well. However, the present theory is elegant to obtain qualitative understanding of solvation time scales and easily adaptable to complicated situations, such as multicomponent systems and the case where solvent is driven out of equilibrium, to name only a few.

Acknowledgment. We thank Professor M. Maroncelli for his critical and helpful comments. R.B. thanks Professor B. M. Deb for his constant encouragement and deep interest in the progress of the above work. Financial assistance from the Department of Science and Technology (DST), India, is gratefully acknowledged.

References and Notes

(1) Bagchi, B. *J. Chem. Phys.* **1994**, *100*, 6658.
(2) Bagchi, B.; Biswas, R. *Adv. Chem. Phys.* **1999**, *109*, 207.
(3) Biswas, R.; Bhattacharyya, S.; Bagchi, B. *J. Chem. Phys.* **1998**, *108*, 4963.
(4) Reynolds, R.; Gardecki, J. A.; Frankland, S. J. V.; Horng, M. L.; Maroncelli, M. *J. Phys. Chem.* **1996**, *100*, 10337.
(5) Ladanyi, B. M.; Nugent, S. *J. Chem. Phys.* **2006**, *124*, 044505.
(6) Egorov, S. A. *Phys. Rev. Lett.* **2004**, *93*, 023004-1.
(7) Egorov, S. A.; Lawrence, C. P.; Skinner, J. L. *J. Phys. Chem. B* **2005**, *109*, 6879.
(8) Aherne, D.; Tran, V.; Schwartz, B. J. *J. Phys. Chem. B* **2000**, *104*, 5382.
(9) Fourkas, J. T.; Benigno, A.; Berg, M. *J. Chem. Phys.* **1993**, *99*, 8552.
(10) Cross, M. C.; Hohenberg, P. *Rev. Mod. Phys.* **1993**, *65*, 851.
(11) Hansen, J. P.; McDonald, I. R. *Theory of Simple Liquids*, 2nd ed.; Academic Press; London, 1986.
(12) Archer, A. J.; Hopkins, P.; Schmidt, M. *Phys. Rev. E* **2007**, *75*, 040501 (R).

(13) Bagchi, B. *Physica A* **1987**, *145*, 273.
(14) Marconi, U. M. B.; Tarazona, P. *J. Chem. Phys.* **1999**, *110*, 8032.
(15) Chakrabarti, J. *J. Chem. Phys.* **2003**, *118*, 249.
(16) The static correlation should be that for the inhomogeneous ground-state solvent distribution involving higher order correlations of the homogeneous solvent. In the absence of the detailed knowledge of the higher order correlations, we include only the second-order correlation.
(17) $\rho_{gs}(\mathbf{r})$ satisfies $\ln[\rho_{gs}(\mathbf{r})/\rho_0] = \int c(\mathbf{r} - \mathbf{r}')[\rho_{gs}(\mathbf{r}') - \rho_0]d\mathbf{r}' - V_{uv}^{gs}(\mathbf{r} - \mathbf{R})$, which has been solved to linear order in $\delta\rho_{gs}(\mathbf{r})$.
(18) Song, W.; Biswas, R.; Maroncelli, M. *J. Phys. Chem. A* **2000**, *104*, 6924.
(19) Peng, D. Y.; Robinson, D. B. *Ind. Eng. Chem. Fundam.* **1976**, *15*, 59.
(20) Frenkel D.; Smit B. *Understanding Molecular Simulation: From Algorithms to Applications*; Academic Press: New York, 1996.
(21) Chialvo, A. A.; Cummings, P. T. *AIChE J.* **1994**, *40*, 1558.
(22) Tucker, S. C. *Chem. Rev.* **1999**, *99*, 391.
(23) Kajimoto, O. *Chem. Rev.* **1999**, *99*, 355.
(24) For $q \approx 0$ and $Q \approx q_0$, $\mathbf{p} \approx \mathbf{Q}$. Integrating over $\chi \in (0,\pi/2)$, one obtains the off-diagonal term. Note that $(\pi - \chi)$ describes the inverse scattering.
(25) Yamaguchi, T.; Kimura, Y.; Nakahara, M. *J. Phys. Chem. B* **2002**, *106*, 9126.
(26) Chialvo, A. A.; Cummings P. T.; Simonson, J. M.; Mesmer, R. E. *J. Chem. Phys*. **1999**, *110*, 1075.
(27) Kometani, N.; Arzhantsev, S.; Maroncelli, M. *J. Phys. Chem. A* **2006**, *110*, 3405.
(28) Kimura, Y.; Hirota, N. *J. Chem. Phys.* **1999**, *111*, 5474.
(29) Kapko, V.; Egorov, S. A. *J. Chem. Phys.* **2004**, *121*, 11145.
(30) Egorov, S. A. *J. Chem. Phys.* **2004**, *121*, 6948.
(31) Egorov, S. A. *J. Chem. Phys.* **2000**, *113*, 1950.
(32) Egorov, S. A. *J. Chem. Phys.* **2002**, *116*, 2004.
(33) Ingrosso, F.; Ladanyi, B. M.; Mennucci, B.; Scalmani, G. *J. Phys. Chem. B* **2006**, *110*, 4953.
(34) Nugent, S.; Ladanyi, B. M. *J. Chem. Phys.* **2004**, *120*, 874.
(35) Ingrosso, F.; Ladanyi, B. M.; Mennucci, B.; Elola, M. D.; Tomasi, J. *J. Phys. Chem. B* **2005**, *109*, 3553.
(36) Ladanyi, B. M.; Maroncelli, M. *J. Chem. Phys.* **1998**, *109*, 3204.
(37) Re, M.; Laria, D. *J. Phys. Chem. B* **1997**, *101*, 10494.
(38) Saven, J. G.; Skinner, J. L. *J. Chem. Phys.* **1993**, *99*, 4391.